Journal of Biomechanics 90 (2019) 65–70

Contents lists available at ScienceDirect

Journal of Biomechanics

journal homepage: www.elsevier.com/locate/jbiomech
www.JBiomech.com

The effects of variation in the arterial pulse waveform on perivascular flow

Robert A. Lloyd [a], Marcus A. Stoodley [b], David F. Fletcher [c], Lynne E. Bilston [a,*]

[a] Neuroscience Research Australia and Prince of Wales Clinical School, University of New South Wales, Australia
[b] Department of Clinical Medicine, Macquarie University, Australia
[c] School of Chemical and Biomolecular Engineering, The University of Sydney, Australia

ARTICLE INFO

Article history:
Accepted 21 April 2019

Keywords:
Syringomyelia
Chiari malformation
Cerebrospinal fluid (CSF)
Perivascular space
Computational fluid dynamics (CFD)

ABSTRACT

Cerebrospinal fluid (CSF) enters nervous tissues through perivascular spaces. Flow through these pathways is important for solute transport and to prevent fluid accumulation. Syringomyelia is commonly associated with subarachnoid space obstructions such as Chiari I malformation. However, the mechanism of development of these fluid-filled cavities is unclear. Studies have suggested that changes in the arterial and CSF pressures could alter normal perivascular flow. This study uses an idealised model of the perivascular space to investigate how variation in the arterial pulse influences fluid flow. The model used simulated subarachnoid pressures from healthy controls (N = 9), Chiari patients with (N = 7) and without (N = 8) syringomyelia. A parametric analysis was conducted to determine how features of the arterial pulse altered flow. The features of interest included: the timing and magnitude of the peak displacement, and the area under the curve in the phases of uptake and decline. A secondary aim was to determine if the previously observed differences between subject groups were sensitive to variation in the arterial pulse wave. The study demonstrated that the Chiari patients without a syrinx maintained a significantly higher level of perivascular inflow over a physiologically likely range of pulse wave shapes. The analysis also suggested that age-related changes in the arterial pulse (i.e. increased late systolic pulse amplitude and faster diastolic decay), could increase resistance to perivascular inflow affecting solute transport.

1. Introduction

The perivascular spaces are fluid channels within the brain and spinal cord which surround arteries and veins (Lam et al., 2017). These structures provide a conduit between the cerebrospinal fluid (CSF) in the subarachnoid space and parenchymal interstitial fluid, facilitating solute transport and waste clearance (Diem et al., 2016; Hawkes et al., 2011; Iliff et al., 2013a). Tracer studies have indicated that arterial pulsations are involved in perivascular transport (Iliff et al., 2013b; Rennels et al., 1985; Stoodley et al., 1997; Stoodley et al., 1999). Identifying the normal function of the perivascular spaces and how flow can be disrupted is vital to understanding healthy neural function, and abnormal fluid accumulation in nervous tissues.

Syrinxes are fluid filled cavities which form in the spinal cord, they are commonly associated with subarachnoid space obstructions. Syrinxes can cause sensory and motor disturbances, and current surgical treatments are frequently unsuccessful (Aghakhani et al., 2009). Fluid accumulation in a syrinx is the net result of an imbalance between fluid inflow and outflow, and since the mechanisms which cause fluid accumulation are unknown, this hinders treatment improvements.

As CSF flow through the perivascular spaces depends on arterial pulsation (Iliff et al., 2013b; Rennels et al., 1985; Stoodley et al., 1997; Stoodley et al., 1999), computational models have been used to explore the biomechanics, showing that arterial pulsation alone cannot actively drive flow in the absence of a pressure gradient (Asgari et al., 2016; Bilston et al., 2003). However, the artery could act as a 'leaky' valve. While an artery expands the perivascular space narrows, increasing resistance to flow driven by dynamic subarachnoid space pressure (Bilston et al., 2010). As such, flow through the perivascular spaces will be related to the timing differences between the arterial and subarachnoid pressures (Clarke et al., 2017; Lloyd et al., 2017).

Lumped parameter models have shown that decreased spinal canal compliance induces a timing shift in the subarachnoid pressures favourable for increased fluid accumulation (Elliott et al., 2011; Martin et al., 2012). Our perivascular space model together with simulated subject-specific pressure data (Lloyd et al., 2017),

* Corresponding author.
E-mail address: L.Bilston@neura.edu.au (L.E. Bilston).

https://doi.org/10.1016/j.jbiomech.2019.04.030
0021-9290/

predicted that the timing changes introduced by Chiari malformation could significantly increase inflow compared with controls.

Research has focused on how changes in subarachnoid pressure influence perivascular flow but not examined how variations in the arterial pulse wave affect flow. The arterial waveform is comprised of the forward and reflected travelling pulse waves (Fig. 1). Reflections are produced by impedance differences along the vascular tree. For further details of what influences the pulse waveform shape, see (Kim et al., 2017; London and Pannier, 2010).

Changes in the arterial waveform may alter perivascular space dimensions across the cardiac cycle, and thus affect the efficiency of the 'leaky valve' mechanism. This study used an idealised model of the perivascular space with subject-specific subarachnoid pressure profiles to assess how features of the arterial pulse waveform influence perivascular flow, in order to determine whether the 'leaky valve' mechanism is sensitive to the arterial pulse waveform. We hypothesised that pulse wave variations within typical physiological ranges would minimally affect net CSF inflow.

2. Methods

2.1. Modelling perivascular flow

A previously published idealised model of the perivascular space was used (Bilston et al., 2010). The model comprises an axisymmetric annulus of fluid surrounding a representative penetrating artery of the spinal cord (Fig. 2). Previously calculated subarachnoid space pressures derived from subject-specific CSF flows for 9 controls, 7 Chiari patients with a syrinx and 8 without (Fig. 2B), were applied to the inlet of the model (Lloyd et al., 2017). The outlet in the cord parenchyma was set at the reference gauge pressure (0 Pa). Arterial expansion was simulated by applying a time-dependent displacement to a moving inner annular wall (Fig. 3A). Since the wavelength of the arterial pulse is orders of magnitude greater than the length of the perivascular space, the displacement was applied uniformly along its length. The soft tissue of the spinal cord (the outer radius) was modelled as a rigid wall boundary, since the cord is nearly incompressible with a Young's modulus (~1 MPa (Bilston and Thibault, 1995)) orders of magnitude greater than the perivascular pressures (<100 Pa).

Systolic uptake was set at 4% of the cardiac cycle, within the range of timing measured in vivo (5 ± 1 of the cardiac cycle) (Lloyd et al., 2017). The model was solved in ANSYS CFX (v17.1, ANSYS Inc, Pittsburgh, PA, USA); the high resolution bounded second order scheme was used for the advection term and the second order backward Euler scheme for the transient term. At each time step the normalised residuals were required to be below 2×10^{-5} for convergence. CSF was modelled as a Newtonian fluid (ν = 0.8 mPa·s, ρ = 1000 kg m^{-3} (Bloomfield et al., 1998)). The flow rate was integrated over the cycle to calculate the net mass flux per cardiac cycle. Positive values indicate net inflow towards the central canal. See Bilston et al. (2010), Clarke et al. (2017) and Lloyd et al. (2017) for further details.

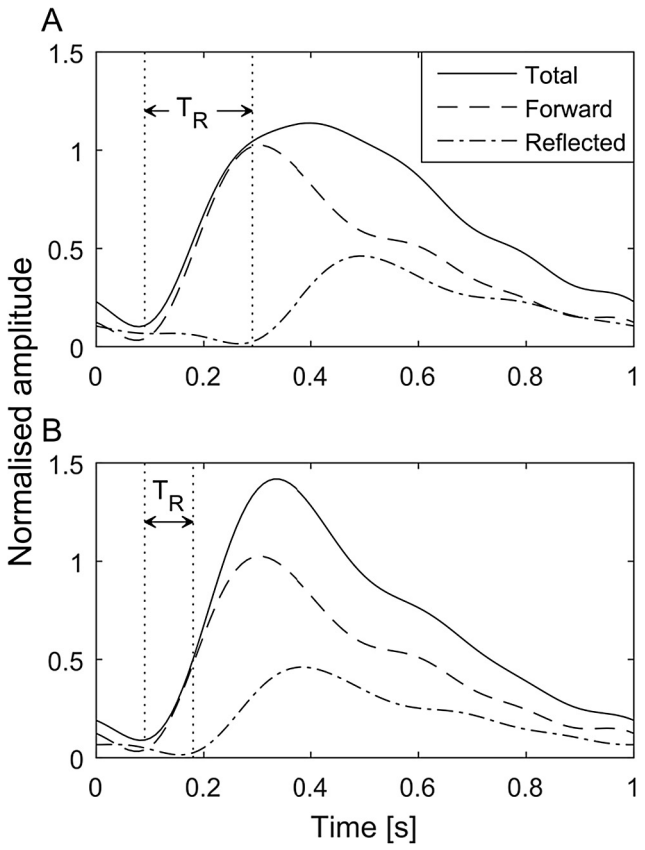

Fig. 1. Illustration demonstrating how the interactions of the forward travelling and reflected waves may alter the shape of the arterial pressure pulse, adapted from London and Pannier (2010). (A) A baseline example with the travel time of the reflected wave (T_R) being 0.29 s. (B) The effects of increasing the stiffness of the aorta, reducing the travelling time of the reflected wave to 0.18 s, shifting the peak into late systole and reducing the diastolic pressure.

2.2. Arterial pulse wave

Parametric analysis was conducted to assess how the arterial waveform affected perivascular flow. A simplified version of the displacement waveform used in Bilston et al. (2010) was used as a baseline (Fig. 3A). Features of the displacement wave were systematically altered to mimic in vivo waveform characteristics, while maintaining the baseline value for remaining features (Fig. 3 and Table 1). Each displacement wave was applied to the model for all 24 subject-specific pressure profiles.

2.2.1. Arterial pulse amplitude

The arterial wall deformation within the spinal cord penetrating arteries is unknown, and an amplitude of 10 μm has been assumed previously (Bilston et al., 2010; Clarke et al., 2017). There, the pulse waveform was scaled to 1.25, 2.5, 5, and 20 μm peak amplitude.

2.2.2. Systolic peak time

Systolic peak timing was shifted by between −18 to +10% from baseline (Fig. 3D; Table 1), to span values in the vertebral artery (first peak = 9 ± 2% and second peak = 25 ± 7% of the cardiac cycle after systolic uptake), and carotid artery (−8 to 5% change from baseline, from the youngest to oldest, respectively) (Kelly et al., 1989). Resulting variation in the total area under the curve (AUC) from baseline was kept below 4%.

2.2.3. Systolic peak time and duration (Area under systolic uptake)

The AUC during systolic uptake was increased from 9 to 35% from baseline, spanning the increase between 30 and 70 years (Kelly et al., 1989), by shifting the systolic peak 8–18% earlier. The peak displacement was maintained until the beginning of systolic decline, which was held at 28% of the cardiac cycle (Table 1). AUC during uptake was not decreased as this would require the wave to be altered in late systole and diastole.

2.2.4. Area under systolic decline and diastolic run-off

The AUC during decline was decreased by 15 to 49% from the baseline, to cover a range of values (−39 to −11% change from

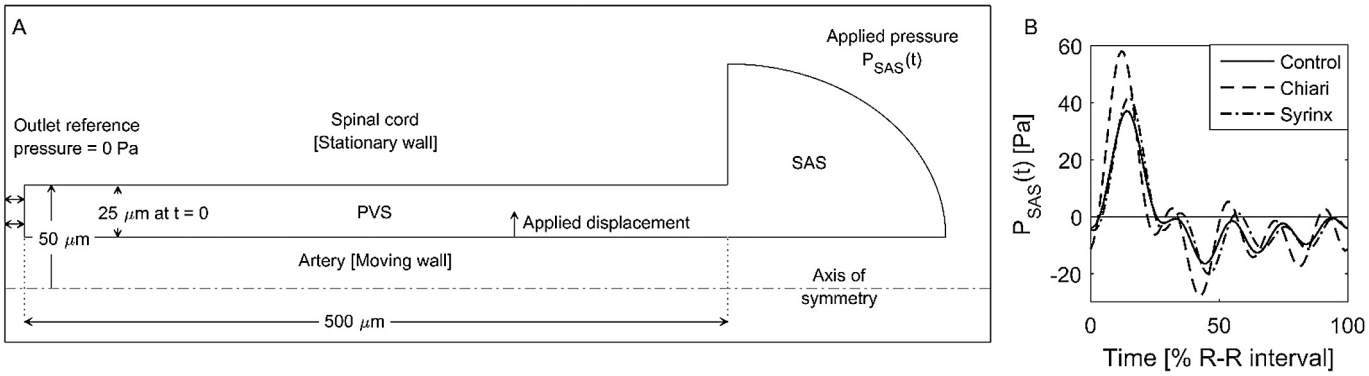

Fig. 2. Annotated schematic of the axisymmetric perivascular space model. Flow within the perivascular space is oscillatory, as such fluid can either flow through the outlet towards the central canal (left on schematic), or return through the outlet towards the subarachnoid space (SAS; right on schematic). The applied pressure $P_{SAS}(t)$ is one of the 24 different subject-specific pressure-time profiles calculated in Lloyd et al. (2017). (B) Shows the ensemble-averaged waveforms for the three subject groups.

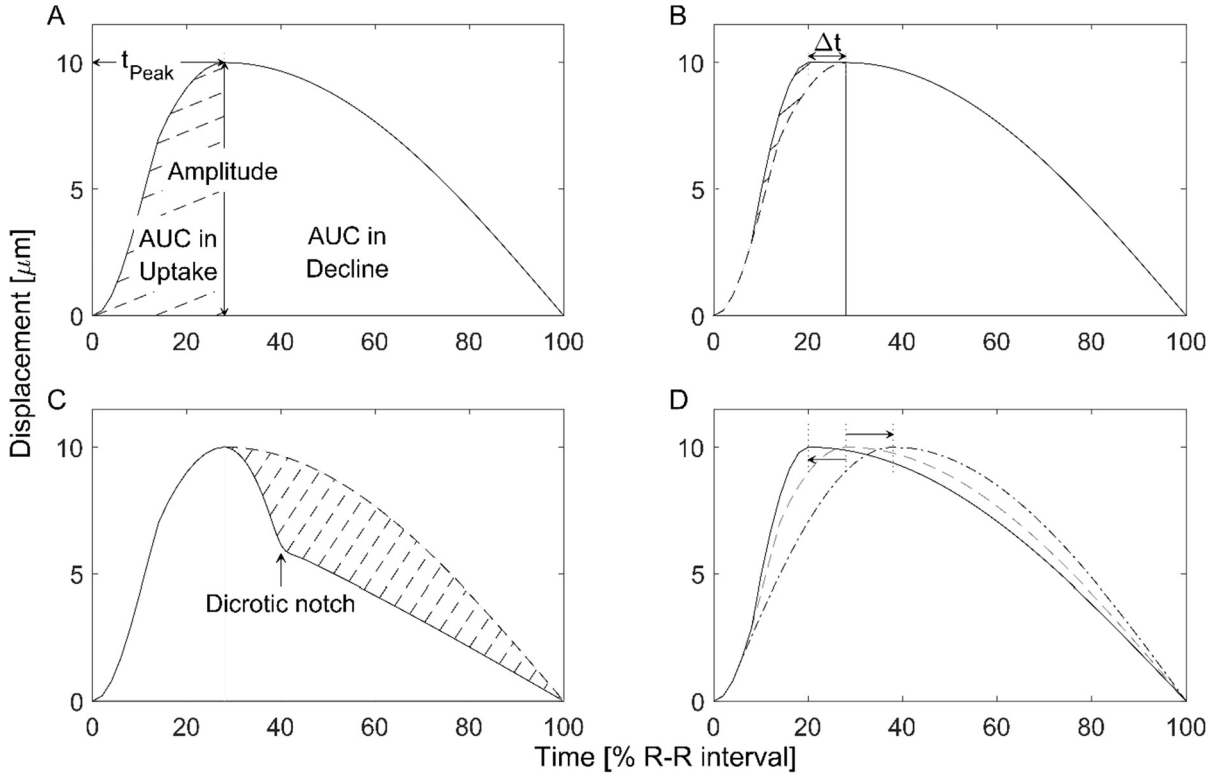

Fig. 3. Example of the arterial displacement waveforms used in the parametric analysis. (A) Annotated baseline waveform, highlight the features of interest in this study. (B) Example of a profile with an earlier peak displacement (t_{peak}) being sustained for a longer time (Δt) (increased AUC in uptake; AUC_{Uptake}). (C) Example of a profile with a rapid decline in pressure during late systole and diastole (decreased AUC in decline; $AUC_{Decline}$), by imposing an artificial dicrotic notch to the waveform at 40% of the cardiac cycle. (D) Example waveforms for changing the time of the peak displacement while keeping the total area the same.

baseline, from the oldest to youngest respectively) estimated from Kelly et al. (1989), by altering the magnitude of the displacement at the dicrotic notch (Fig. 3C). The dicrotic notch was assumed to occur at 40% of the cardiac cycle (38 ± 8% of the cardiac cycle in vertebral artery profiles).

2.3. Statistical analysis

The effect of arterial waveform on net perivascular flow was assessed using a generalised linear mixed model (GLMM) with Bonferroni correction (IBM Statistics v24, IBM Corp., Armonk, NY). $p < 0.05$ was considered significant.

3. Results

Fig. 4 shows the effect of the arterial wave variations on net perivascular inflow. Fig. 4A shows that reducing the pulse amplitude decreases the net inflow. Conversely, increasing the amplitude slightly increased CSF inflow. Earlier arrival of the systolic peak reduces CSF flow into the spinal cord (Fig. 4B). Perivascular flow decreased with increasing AUC during systolic uptake (Fig. 4C), and decreased AUC during systolic decline and diastole (Fig. 4D).

In controls, there was net outflow of fluid when either; the systolic peak times were earlier than 14% of the cardiac cycle, the AUC

Table 1
Alterations made to displacement wave, displayed as: variable value (percentage change from baseline model). Highlighted cells indicate variables altered, where AUC_{Uptake} is the area under the curve during systolic uptake, $AUC_{Decline}$ is the area under the curve during sytolic decline and diastole, and t_{peak} is the time when peak displacement occurs.

Wave Name	Amplitude [μm (% change)]	Peak time [% R-R interval (% change)]	Peak duration (Δt) [% R-R interval (% change)]	AUC in uptake [μm (% change)]	AUC in Decline [μm (% change)]	Total AUC [μm (% change)]
Baseline	10	28	0	1.62	4.3	5.93
Amp 1.25μm	1.25 (−87.5)	28	0	0.20 (−87.5)	0.50 (−87.5)	0.74 (−87.5)
Amp 2.5 μm	2.5 (−75)	28	0	0.40 (−75.0)	1.10 (−75.0)	1.48 (−75.0)
Amp 5 μm	5 (−50)	28	0	0.81 (−50.0)	2.20 (−50.0)	2.96 (−50.0)
Amp 20 μm	20 (100)	28	0	3.23 (100)	8.60 (100)	11.9 (100)
AUC_{Uptake} +9%	10	20 (−8.0)	8 (8.0)	1.75 (8.52)	4.30	6.07 (2.32)
AUC_{Uptake} +21%	10	14 (−14)	14 (14)	1.96 (21.0)	4.30	6.27 (5.73)
AUC_{Uptake} +35%	10	10 (−18)	18 (18)	2.18 (34.9)	4.30	64.9 (9.51)
$AUC_{Decline}$ −49%	10	28	0	1.62	2.20 (−49.0)	3.81 (-35.7)
$AUC_{Decline}$ −33%	10	28	0	1.62	2.90 (−32.8)	4.52 (-23.8)
$AUC_{Decline}$ −15%	10	28	0	1.62	3.70 (−14.9)	5.29 (-10.8)
t_{Peak} −18%	10	10 (−18)	0	0.40 (−75.0)	5.60 (30.9)	6.05 (2.03)
t_{Peak} −14%	10	14 (−14)	0	0.59 (−63.3)	5.40 (24.9)	5.98 (0.85)
t_{Peak} −8%	10	20 (−8)	0	0.97 (−39.7)	5.00 (16.1)	5.98 (0.87)
t_{Peak} +10%	10	38 (10)	0	2.26 (39.5)	3.90 (-9.98)	6.14 (3.52)

during systolic uptake was increased more than 26%, or the AUC during systolic decline and diastole was decreased more than 23%. Chiari patients without a syrinx maintained a significantly greater influx of CSF compared with controls and syrinx patients for all conditions. However, for amplitudes <5 μm and systolic peaks occurring earlier than 14% into the cardiac cycle, the 95% confidence intervals overlap.

There were no interaction effects between the subject groups and the characteristics of the arterial pulse wave (GLMM: Amplitude; $p = 0.146$, AUC uptake; $p = 0.455$, AUC decline; $p = 0.959$, systolic peak time; $p = 0.65$). Therefore, differences between groups can be attributed to differences in the input subarachnoid pressures.

4. Discussion

4.1. Influence of arterial pulse waveform on the 'leaky valve' mechanism

These models suggest that the 'leaky valve' mechanism is relatively unaffected by physiological variations in the arterial pulse waveform. While the 'leaky valve' mechanism is most sensitive to changes in the timing of the systolic peak, a major reduction in perivascular flow requires an unphysiologically early systolic peak (Kelly et al., 1989). Chiari subjects had a significantly higher inflow over a physiologically likely range of parameters (Fig. 4).

Our wave amplitude results are in agreement with previous animal studies showing that diminished arterial pulse amplitude reduces CSF tracer penetration into the spinal cord (Stoodley et al., 1997; Stoodley et al., 1999). Given the relative timing of the CSF and arterial pulses, the positive pressure that drives CSF into the spinal cord occurs during a period of low resistance (late diastole – early systole), whereas the backflow driven by the negative pressures faces the largest resistance due to arterial expansion. Therefore, the reduced perivascular flow seen at low amplitude can be attributed to increased backflow. Conversely, increasing the amplitude above 10 μm also increased resistance to inflow, causing a minimal increase in CSF inflow (Fig. 4A). The sensitivity to the timing of the peak displacement (Fig. 4B), is similarly affected by the change to inflow resistance.

The low impedance of the cerebral vascular bed (Kim et al., 2017) allows for small penetrating arteries to maintain pulsatile pressures (Blanco et al., 2017; Geurts et al., 2018). As such, the pressure waveform would likely have a pronounced peak in systole, with a gradual decline through late systole and diastole. Measurements from the vertebral and carotid artery (Kelly et al., 1989) suggest that the baseline waveform (Fig. 3A) used in previous studies (Bilston et al., 2010; Clarke et al., 2017; Lloyd et al., 2017) may overestimate the efficiency of the 'leaky valve' mechanism (Fig. 4D). However, group differences between Chiari subjects and controls are not altered (Fig. 4), suggesting that the 'leaky valve' is robust to physiologically reasonable variations in the arterial pulse waveform.

4.2. Study limitations

The subarachnoid pressures were based on cardiac-gated MRI scans, neglecting any effects of respiration (Hamer et al., 1977; Yildiz et al., 2017). If respiration alters the net subarachnoid pressures, fluid inflow could vary with the respiratory cycle and this should be included in future studies.

In part, spinal subarachnoid flow is driven by arterial pulsation within the cranium (Alperin et al., 2005a; Alperin et al., 2005b). Therefore, changes in the arterial pulse may also affect the subarachnoid pulse shape, which has not been considered here as these effects are not known.

The presence of a syrinx has been repeatedly shown to normalise CSF dynamics (Cirovic and Kim, 2012; Clarke et al., 2013; Elliott et al., 2011; Lloyd et al., 2017; Martin et al., 2010; Martin and Loth, 2009), but there is no in vivo data for perivascular flow. Therefore, perivascular flow arising from CSF pressures in syrinx patients would be expected to be similar to control subjects, as found here and by Lloyd et al. (2017). However, the CSF dynamics in the pre-syrinx state are unknown, so this study uses the syrinx free subjects as an approximation of that initial state, although there are likely differences as these subjects have not yet developed a syrinx. It was not possible to obtain longitudinal clinical or imaging data to confirm this. It follows from this that these results do not provide a complete picture of the mechanisms of syrinx formation or enlargement, as they are based on cross-sectional data. Future studies should address this issue.

This model neglected variation in cross-sectional area and the bundles of collagen fibres found in the perivascular space (Lam

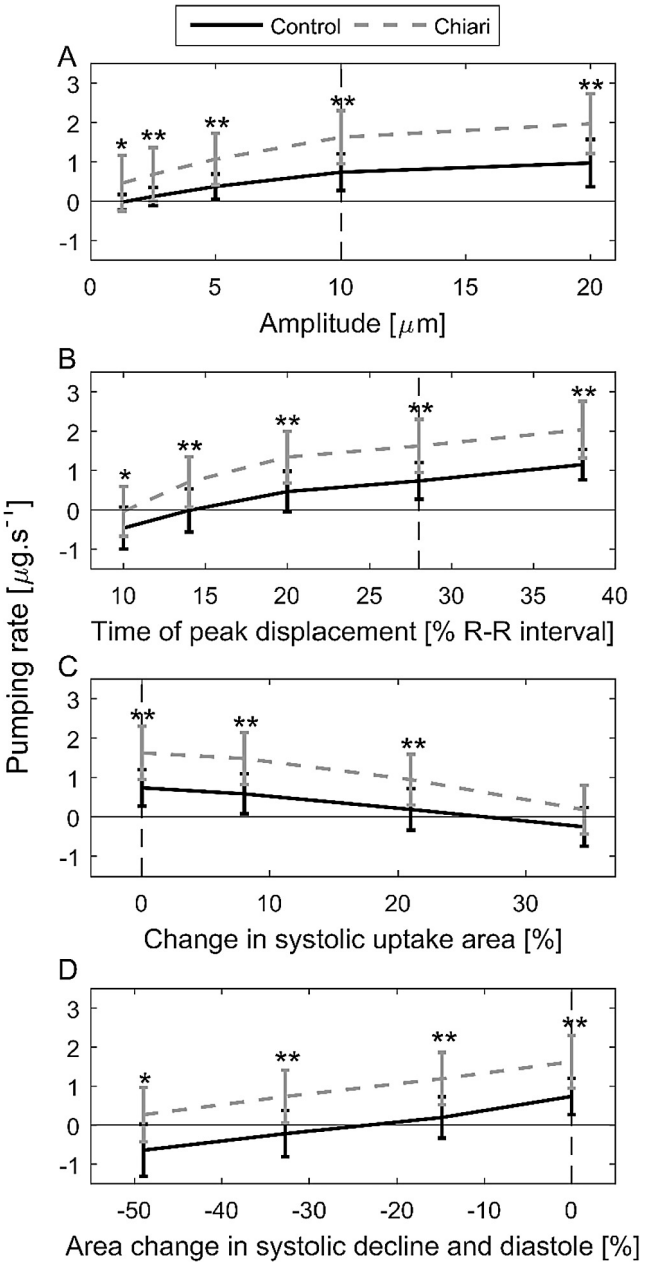

Fig. 4. Calculated pumping rates. Group means with 95% confidence intervals are shown. The pumping rates were calculated by varying the following parameters from the baseline value; (A) arterial expansion amplitude, (B) area during systolic uptake, (C) area during systolic decline and diastole, (D) the timing of the peak displacement. Dashed vertical line indicates the baseline results. Syrinx patient results removed for clarity as they superimpose the control results. Significant comparisons are indicated by an asterisk (* = $p < 0.05$, ** = $p < 0.001$).

et al., 2017). The models may thus underestimate perivascular resistance to flow.

We did not model temporal variation in the internal pressure of the spinal cord, effectively assuming the cord pressure curve follows the caudal subarachnoid pressure. A syrinx would elevate the pressure within the spinal cord, either in or out of phase with the subarachnoid pressure (Heiss et al., 1999), altering the pressure gradient and reducing perivascular flow. This would have a comparable effect to altering the shape of the subarachnoid pressure waveform in isolation, the effects of which has been explored by Clarke et al. (2017).

Solute transport has not explicitly been simulated in this study. However, tracer particles such as Ovalbumin (Tao and Nicholson, 1996) would be dominated by convective flow (Péclet number ≈ 1250, for a typical 5 mm·s^{-1} velocity) and closely follow bulk flow, as seen in recent intravital imaging studies (Bedussi et al., 2018; Mestre et al., 2018). Modelling particle deposition or flow into the parenchyma should be a focus of future work.

5. Conclusion

In this parametric analysis, it has been demonstrated that Chiari patients without a syrinx maintain a significantly greater perivascular flow into the cord over a physiologically realistic range of arterial pulse wave shapes, indicating that the error introduced using idealised arterial pulse shapes in previous studies is likely to be small. The results also suggest that changes in the arterial pulse associated with aging (i.e. increased late systolic pulse amplitude and faster diastolic decay) may slightly decrease perivascular flow.

Acknowledgements

The authors wish to thank Barbara Toson for providing advice for the statistical analysis. This research was funded by the Column of Hope (USA) and NHMRC project grant #1063628 (Australia). Lynne E. Bilston is supported by a NHMRC Senior Research Fellowship.

Conflicts of interest

No conflicts of interest to declare.

References

Aghakhani, N., Parker, F., David, P., Morar, S., Lacroix, C., Benoudiba, F., Tadie, M., 2009. Long-term follow-up of Chiari-related syringomyelia in adults: analysis of 157 surgically treated cases. Neurosurgery 64, 308–315. discussion 315.

Alperin, N., Hushek, S.G., Lee, S.H., Sivaramakrishnan, A., Lichtor, T., 2005a. MRI study of cerebral blood flow and CSF flow dynamics in an upright posture: the effect of posture on the intracranial compliance and pressure. Acta Neurochirurg. Suppl. 95, 177–181.

Alperin, N., Sivaramakrishnan, A., Lichtor, T., 2005b. Magnetic resonance imaging—based measurements of cerebrospinal fluid and blood flow as indicators of intracranial compliance in patients with Chiari malformation. J. Neurosurg. 103, 46–52.

Asgari, M., de Zelicourt, D., Kurtcuoglu, V., 2016. Glymphatic solute transport does not require bulk flow. Sci. Rep. 6, 38635.

Bedussi, B., Almasian, M., de Vos, J., VanBavel, E., Bakker, E.N., 2018. Paravascular spaces at the brain surface: Low resistance pathways for cerebrospinal fluid flow. J. Cereb. Blood Flow Metabol.: Off. J. Int. Soc. Cereb. Blood Flow Metabol. 38, 719–726.

Bilston, L.E., Fletcher, D.F., Brodbelt, A.R., Stoodley, M.A., 2003. Arterial pulsation-driven cerebrospinal fluid flow in the perivascular space: a computational model. Comput. Methods Biomech. Biomed. Eng. 6, 235–241.

Bilston, L.E., Stoodley, M.A., Fletcher, D.F., 2010. The influence of the relative timing of arterial and subarachnoid space pulse waves on spinal perivascular cerebrospinal fluid flow as a possible factor in syrinx development. J. Neurosurg. 112, 808–813.

Bilston, L.E., Thibault, L.E., 1995. The mechanical properties of the human cervical spinal cordIn Vitro. Ann. Biomed. Eng. 24, 67–74.

Blanco, P.J., Müller, L.O., Spence, J.D., 2017. Blood pressure gradients in cerebral arteries: a clue to pathogenesis of cerebral small vessel disease. Stroke Vasc. Neurol. 2, 108–117.

Bloomfield, I.G., Johnston, I.H., Bilston, L.E., 1998. Effects of proteins, blood cells and glucose on the viscosity of cerebrospinal fluid. Pediat. Neurosurg. 28, 246–251.

Cirovic, S., Kim, M., 2012. A one-dimensional model of the spinal cerebrospinal-fluid compartment. J. Biomech. Eng. 134, 021005.

Clarke, E.C., Fletcher, D.F., Bilston, L.E., 2017. Sustained high-pressure in the spinal subarachnoid space while arterial expansion is low may be linked to syrinx development. Comput. Methods Biomech. Biomed. Eng. 20, 457–467.

Clarke, E.C., Stoodley, M.A., Bilston, L.E., 2013. Changes in temporal flow characteristics of CSF in Chiari malformation Type I with and without syringomyelia: implications for theory of syrinx development. J. Neurosurg. 118, 1135–1140.

Diem, A.K., Tan, M., Bressloff, N.W., Hawkes, C., Morris, A.W.J., Weller, R.O., Carare, R. O., 2016. A simulation model of periarterial clearance of amyloid-β from the brain. Front. Aging Neurosci., 8

Elliott, N., Lockerby, D.A., Brodbelt, A., 2011. A lumped-parameter model of the cerebrospinal system for investigating arterial-driven flow in posttraumatic syringomyelia. Med. Eng. Phys. 33, 874–882.
Geurts, L., Biessels, G.J., Luijten, P., Zwanenburg, J., 2018. Better and faster velocity pulsatility assessment in cerebral white matter perforating arteries with 7T quantitative flow MRI through improved slice profile, acquisition scheme, and postprocessing. Magn. Reson. Med. 79, 1473–1482.
Hamer, J., Alberti, E., Hoyer, S., Wiedemann, K., 1977. Influence of systemic and cerebral vascular factors on the cerebrospinal fluid pulse waves. J. Neurosurg. 46, 36–45.
Hawkes, C.A., Hartig, W., Kacza, J., Schliebs, R., Weller, R.O., Nicoll, J.A., Carare, R.O., 2011. Perivascular drainage of solutes is impaired in the ageing mouse brain and in the presence of cerebral amyloid angiopathy. Acta Neuropathol. 121, 431–443.
Heiss, J.D., Patronas, N., DeVroom, H.L., Shawker, T., Ennis, R., Kammerer, W., Eidsath, A., Talbot, T., Morris, J., Eskioglu, E., Oldfield, E.H., 1999. Elucidating the pathophysiology of syringomyelia. J. Neurosurg. 91, 553–562.
Iliff, J.J., Lee, H., Yu, M., Feng, T., Logan, J., Nedergaard, M., Benveniste, H., 2013a. Brain-wide pathway for waste clearance captured by contrast-enhanced MRI. J. Clin. Invest. 123, 1299–1309.
Iliff, J.J., Wang, M., Zeppenfeld, D.M., Venkataraman, A., Plog, B.A., Liao, Y., Deane, R., Nedergaard, M., 2013b. Cerebral arterial pulsation drives paravascular CSF-interstitial fluid exchange in the murine brain. J. Neurosci. 33, 18190–18199.
Kelly, R., Hayward, C., Avolio, A., O'Rourke, M., 1989. Noninvasive determination of age-related changes in the human arterial pulse. Circulation 80, 1652–1659.
Kim, M.O., Li, Y., Wei, F., Wang, J., O'Rourke, M.F., Adji, A., Avolio, A.P., 2017. Normal cerebral vascular pulsations in humans: changes with age and implications for microvascular disease. J. Hypertens. 35, 2245–2256.
Lam, M.A., Hemley, S.J., Najafi, E., Vella, N.G.F., Bilston, L.E., Stoodley, M.A., 2017. The ultrastructure of spinal cord perivascular spaces: Implications for the circulation of cerebrospinal fluid. Sci. Rep. 7, 12924.
Lloyd, R.A., Fletcher, D.F., Clarke, E.C., Bilston, L.E., 2017. Chiari malformation may increase perivascular cerebrospinal fluid flow into the spinal cord: a subject-specific computational modelling study. J. Biomech. 65, 185–193.
London, G.M., Pannier, B., 2010. Arterial functions: how to interpret the complex physiology. Nephrol. Dial. Transplant. 25, 3815–3823.
Martin, B.A., Labuda, R., Royston, T.J., Oshinski, J.N., Iskandar, B., Loth, F., 2010. Spinal subarachnoid space pressure measurements in an in vitro spinal stenosis model: implications on syringomyelia theories. J. Biomech. Eng. 132, 111007.
Martin, B.A., Loth, F., 2009. The influence of coughing on cerebrospinal fluid pressure in an in vitro syringomyelia model with spinal subarachnoid space stenosis. Cerebrospinal Fluid Res. 6, 17.
Martin, B.A., Reymond, P., Novy, J., Balédent, O., Stergiopulos, N., 2012. A coupled hydrodynamic model of the cardiovascular and cerebrospinal fluid system. Am. J. Physiol.-Heart Circul. Physiol. 302, H1492–H1509.
Mestre, H., Tithof, J., Du, T., Song, W., Peng, W., Sweeney, A.M., Olveda, G., Thomas, J. H., Nedergaard, M., Kelley, D.H., 2018. Flow of cerebrospinal fluid is driven by arterial pulsations and is reduced in hypertension. Nat. Commun. 9, 4878.
Rennels, M.L., Gregory, T.F., Blaumanis, O.R., Fujimoto, K., Grady, P.A., 1985. Evidence for a 'paravascular' fluid circulation in the mammalian central nervous system, provided by the rapid distribution of tracer protein throughout the brain from the subarachnoid space. Brain Res. 326, 47–63.
Stoodley, M.A., Brown, S.A., Brown, C.J., Jones, N.R., 1997. Arterial pulsation-dependent perivascular cerebrospinal fluid flow into the central canal in the sheep spinal cord. J. Neurosurg. 86, 686–693.
Stoodley, M.A., Gutschmidt, B., Jones, N.R., 1999. Cerebrospinal fluid flow in an animal model of noncommunicating syringomyelia. Neurosurgery 44, 1065–1075. discussion 1075–1066.
Tao, L., Nicholson, C., 1996. Diffusion of albumins in rat cortical slices and relevance to volume transmission. Neuroscience 75, 839–847.
Yildiz, S., Thyagaraj, S., Jin, N., Zhong, X., Heidari Pahlavian, S., Martin, B.A., Loth, F., Oshinski, J., Sabra, K.G., 2017. Quantifying the influence of respiration and cardiac pulsations on cerebrospinal fluid dynamics using real-time phase-contrast MRI. J. Magn. Reson Imag.: JMRI 46, 431–439.